A low-Reynolds-number, high-angle-of-attack investigation of wind turbine aerofoils

S Worasinchai, G Ingram and R Dominy

Proceedings of the Institution of Mechanical Engineers, Part A: Journal of Power and Energy 2011 225: 748 originally published online 18 July 2011
DOI: 10.1177/0957650911405411

A low-Reynolds-number, high-angle-of-attack investigation of wind turbine aerofoils

S Worasinchai*, **G Ingram,** and **R Dominy**
School of Engineering and Computing Sciences, Durham University, Durham, UK

The manuscript was received on 7 December 2010 and was accepted after revision for publication on 9 March 2011.

DOI: 10.1177/0957650911405411

Abstract: This article describes an experimental, aerodynamic investigation of four aerofoils intended for small wind turbine applications. The aerofoils of these small machines (both horizontal and vertical axes) normally experience conditions that are quite different from large-scale machines due to smaller chord length and lower wind speed, resulting in significantly lower Reynolds numbers. They also operate with an unusually wide range of incidence angles (0° to 90° for horizontal axis and 0° to 360° for vertical axis). Four appropriate aerofoils were chosen for testing at three Reynolds numbers (65 000, 90 000, and 150 000) through 360° incidence to cover almost all possible conditions that might be encountered by both types of turbines. The investigations were conducted in terms of lift, drag, and surface static pressure coefficients. The experimental results show that both geometry and Reynolds number had significant effects on aerodynamic lift, not only when unstalled but particularly in the post-stall region from 20° to 50° incidence. These effects were also seen at other incidences but to a lesser extent. By contrast, the drag characteristics were similar for all blade geometries. Static pressure measurement revealed that, at these low Reynolds numbers, separation bubbles always form near the leading edge of the suction surface at moderate incident angles and increase in size with decreasing Reynolds number. Comparisons of force and static pressure measurements showed that the aerofoil stalling behaviour is closely related to the presence of a separation bubble at the leading edge of the suction surface. Discrepancies between the experiments and predictions using the AERODAS model confirm the continued need for accurate wind tunnel testing.

Keywords: aerofoil, experiment, high angle of attack, low Reynolds number, small wind turbine

1 INTRODUCTION

Wind turbine performance can normally be predicted through the use of blade element momentum theory together with two-dimensional (2-D) aerofoil data [**1**, **2**]. Because of its ability to predict accurate results and its simplicity, this method has been implemented in many performance analysis codes [**3**–**5**]. Wind tunnel or computational fluid dynamics (CFD) derived aerodynamic data is the basic information that has to be provided to these codes. It has been shown that poor quality data can lead to a significant error in power prediction [**6**–**8**].

The data required by performance prediction codes must cover a suitable Reynolds number range for the full 360° range of angle of incidence that is likely to be experienced, including both unstalled and stalled conditions. Unfortunately, this kind of information is scarce and the most available aerofoil data cover only angles of attack up to or just past the stall point. Consequently, estimation often has to be used in order to extrapolate these data to higher angles of attack.

The estimation is normally done through the application of flat plate theory or empirical correlations [**9**–**12**]. In flat plate theory, all aerofoils are assumed

**Corresponding author: School of Engineering and Computing Sciences, Durham University, South Road, Durham DH1 3LE, UK. email: supakit.worasinchai@durham.ac.uk*

to behave like a flat plate and, hence, their post-stall characteristics are independent of their shape and Reynolds number. Nevertheless, high-angle-of-attack tests on some real aerofoils has revealed that different aerofoils may demonstrate significantly different characteristics from each other even when fully stalled [**13–15**], thus casting doubt on the validity of the flat plate assumption.

Wind tunnel based correlations have also been developed to predict aerodynamic coefficients at high incidence angles, including the empirical correlations developed by Spera (AERODAS) [**12**]. In his correlation process, selected aerofoils data at high angle of attack in a Reynolds number range from 250 000 to 2 000 000 were analysed and modelled in order to obtain expressions for aerodynamic coefficient prediction. Although the correlations provide useful information for wind turbine analysis, it is questionable whether it is possible to apply this to other aerofoils or to conditions outside this Reynolds number range, especially lower Reynolds number.

The starting performance of a small horizontal axis turbine has been experimentally investigated and modelled by Wright and Wood [**16**]. However, due to a lack of aerofoil data at low Reynolds numbers and high angles of incidence, three estimated sets of aerofoil lift and drag data at a high incident angle had been used. The first set was constructed by combining pre-stall characteristics of their SD7062 aerofoil to the post-stall characteristics of NACA4412 at the lowest Reynolds number for which data were available (250 000). The second post-stall data was obtained using flat plate theory. The third set was an average of the first two. It was found that the accuracy of the predictions varied greatly with the aerofoil data used. While the C_l and C_d from the flat plate theory under-predicted the experimentally observed turbine rotational speed, the combined set gave an over-prediction. The average set fortuitously gave the best agreement with the experimental results. The results clearly stress the importance of reliable data for small wind turbine analysis.

Not only are appropriate data scarce but those data that are available are also frequently found to be inconsistent, especially in the post-stall region. It has been suggested that this is a consequence of the different wind tunnel configurations that have been adopted by different researchers; a hypothesis that is supported by the wind tunnel measurements of Rainbird [**17**]. He demonstrated that if a closed test section is used, the flow around the aerofoil at high incidence angles will be influenced by wall proximity, resulting in an exaggerated negative pressure on the suction side and an increase in lift. The increase in lift can also be seen as analogous to the enhanced lift that is encountered by a wing in ground effect on landing [**18**]. Rainbird [**17**] and Hill [**8**] firmly indicated that the configuration of the wind tunnel section has a crucial influence on aerofoil aerodynamic data and suggested that in order to avoid any possible wall effects at high incidences, a half-open test section should be used.

The main purpose of this article is to investigate experimentally the aerodynamic performance of appropriate aerofoils at low Reynolds numbers through the full incidence range of 360°. These aerodynamic coefficients will serve as a useful information for future small turbine analysis and design.

2 EXPERIMENT

The four aerofoils selected for this study were NACA0012, SG6043, SD7062, and DU06-W-200. Their profiles are depicted in Fig. 1.

NACA0012: The benchmark NACA0012 aerofoil is a symmetrical aerofoil with thickness-to-chord ratio of 12 per cent. It was chosen for testing because it is one of very few aerofoils for which wind tunnel data for the entire range of incidence is available from other authors [**19**].

SG6043: The SG6043 was developed by Selig and Giguere for small variable-speed wind turbines with a rated power of 1–5 kW [**20**]. It was designed for operational Reynolds number of around 300 000. It is a 10 per cent thickness aerofoil with a camber of 5.5 per cent.

SD7062: This profile was designed by Selig and Donovan for aircraft applications [**21**]. Its high lift and soft stall behaviour make it applicable to applications such as small wind turbines and unmanned aerial vehicles (UAVs) as well as aeroplanes. Its thickness-to-chord ratio and camber are 14 per cent and 4 per cent, respectively.

DU06-W-200: This aerofoil was designed by Claessens [**22**] in 2006, intended for use with vertical-axis wind turbines (VAWTs). In this design, a NACA0018 section, which is commonly employed in VAWTs, was modified to improve its performance for turbine application. Thickness (20 per cent) and

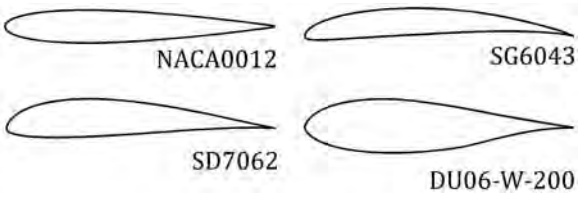

Fig. 1 Tested aerofoils

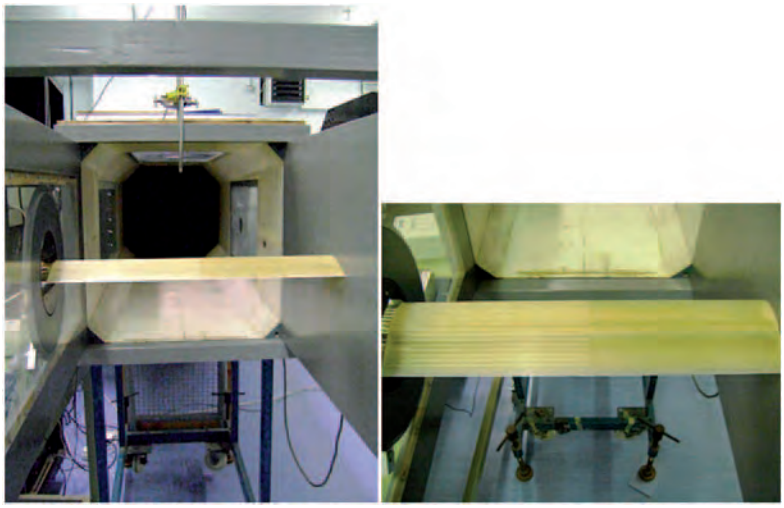

Fig. 2 Test section

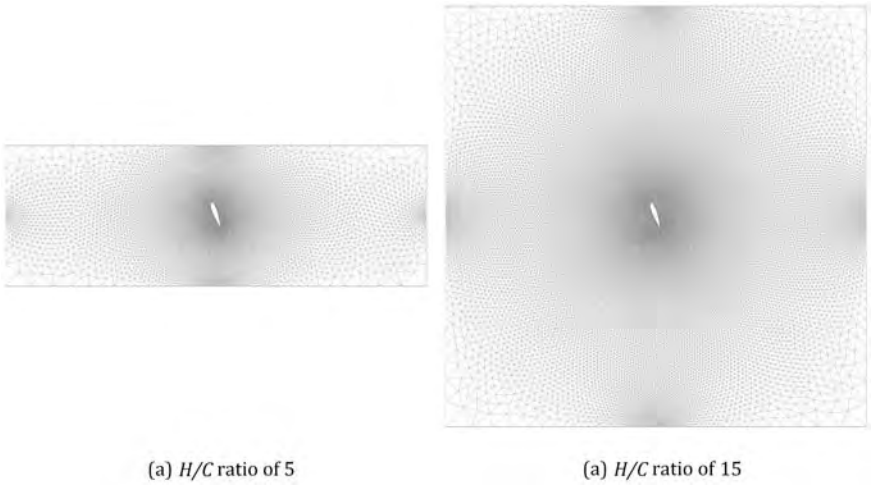

Fig. 3 Computational domains for different height-to-chord ratios

camber (5 per cent) had been added for blade strength and improved aerodynamic characteristics, respectively. However, performance data were only obtained at Reynolds numbers between 300 000 and 500 000. Knowledge of its performance at low Reynolds number is essential for the understanding of its starting capability and low-speed performance.

The wind tunnel used for the experiments presented here was the 0.5-m Plint wind tunnel at Durham University; an open circuit design which discharges directly to the atmosphere. For this investigation, the wind tunnel working section was configured to have a square cross-section (457 mm × 457 mm) with solid sides but open top and bottom (Fig. 2) as recommended by Rainbird [**17**].

In order to clearly demonstrate the effect of the test section configuration when testing at high angles of incidence and to confirm Rainbird's [**17**] finding, CFD calculations of flow around a NACA0012 aerofoil in closed and half-open test sections at different height-to-chord ratios were performed.

The CFD modelling was performed using FLUENT 6.3.26. Two computational domains were created to simulate the wind tunnel test section having different height-to-chord ratios (Fig. 3). Both domains were extended 7.5 chords upstream and downstream. Different height-to-chord ratios were obtained by extending the domain above and below the aerofoil in such a way that the aerofoil was located at the centre of the airstream. This configuration resulted in the computational domain extending 2.5 and 7.5 chords above and below the aerofoil for height-to-chord ratios of 5 and 15, respectively, which led to 2-D, unstructured mesh sizes of 0.0011 m^2 for both domains. The resulting number of cells were approximately 27 000 and 73 000, respectively.

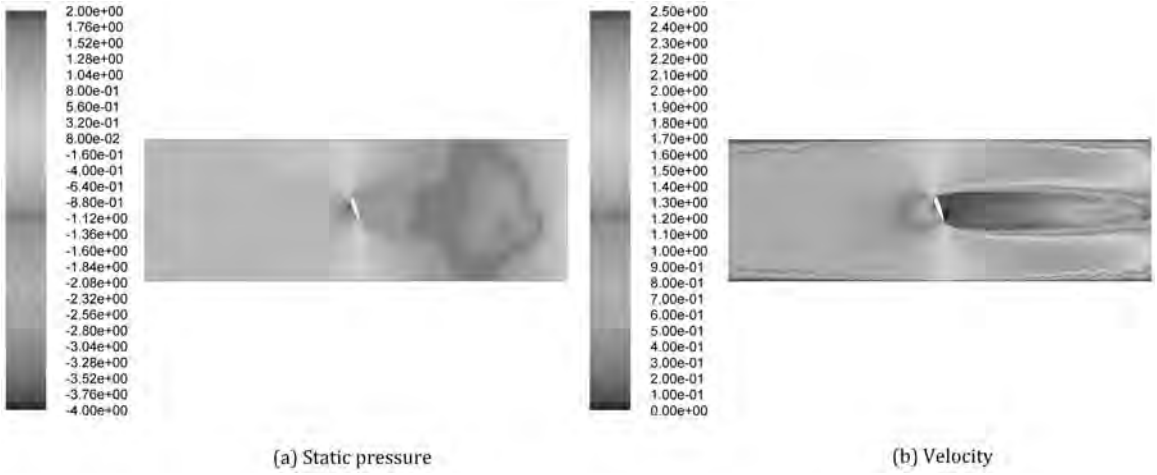

Fig. 4 Flow around a NACA section at $H/C = 5$ and AoA of 70° (closed)

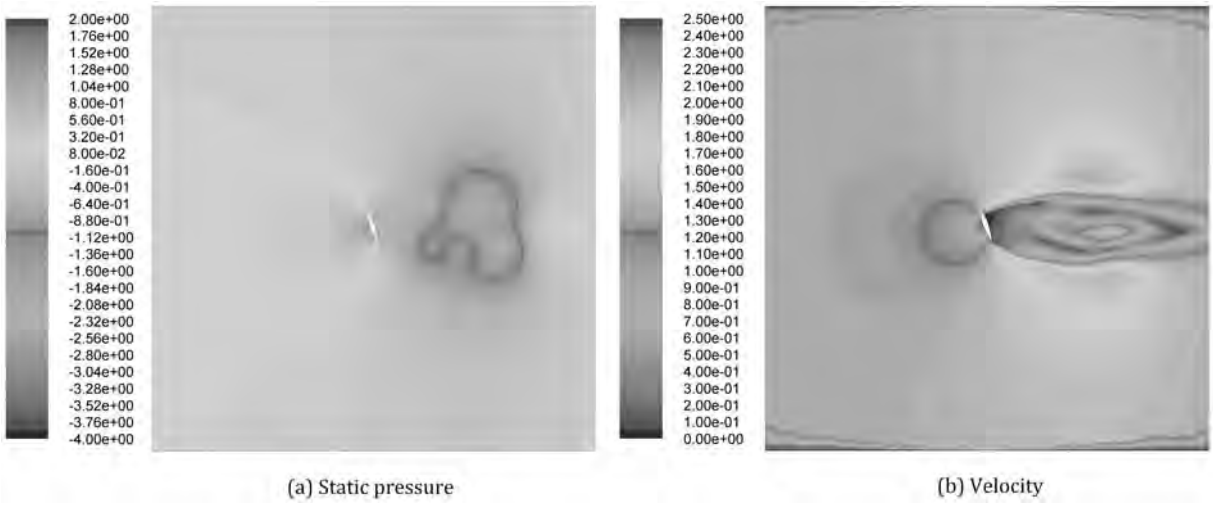

Fig. 5 Flow around a NACA section at $H/C = 15$ and AoA of 70° (closed)

The effects of wall proximity were investigated by changing boundary conditions at the upper and lower domain boundaries which were defined as walls and pressure outlets for the closed and half-open test sections. A laminar flow model was adopted for all simulations since it has been reported that the flow with a Reynolds number lower than 200 000 is extensively laminar [**23**].

Static pressure distributions and velocity distributions for a NACA0012 section in a closed test section are presented with different height-to-chord ratios (Figs 4 and 5).

Comparisons between the two test cases clearly demonstrates the effect of changing the test section's height-to-chord ratio from $H/C = 5$ (Fig. 4) to $H/C = 15$ (Fig. 5) where, in particular, the development of the blade's wake structure is inhibited at the lower H/C ratio by the proximity of the upper and lower walls. For most wind tunnels, significant changes of their working section aspect ratio to accommodate high incidence aerofoil testing are not a viable option.

Similar improvement can be achieved by removing the top and the bottom walls and results for this 'half-open' configuration for the same jet aspect ratios are shown in Figs 6 and 7.

For the larger jet area, the results are almost identical to those of the closed section, but for the smaller jet, the flow is dramatically improved by the adoption of the half-open configuration. CFD derived surface static pressure coefficients around the aerofoil inclined at 70° for both closed and half-open test sections at the different height-to-chord ratios are presented in Fig. 8 together with pressure coefficients in an infinite jet ($H/C =$ infinity).

It is clear that at this high angle of attack, there is very little difference on either surface of the aerofoil

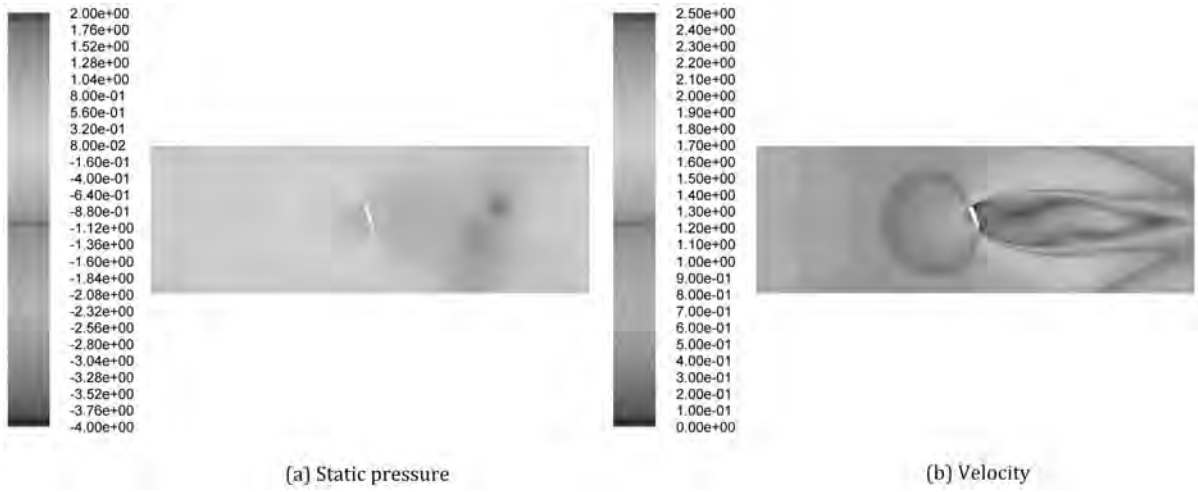

Fig. 6 Flow around a NACA section at $H/C = 5$ and AoA of 70° (open)

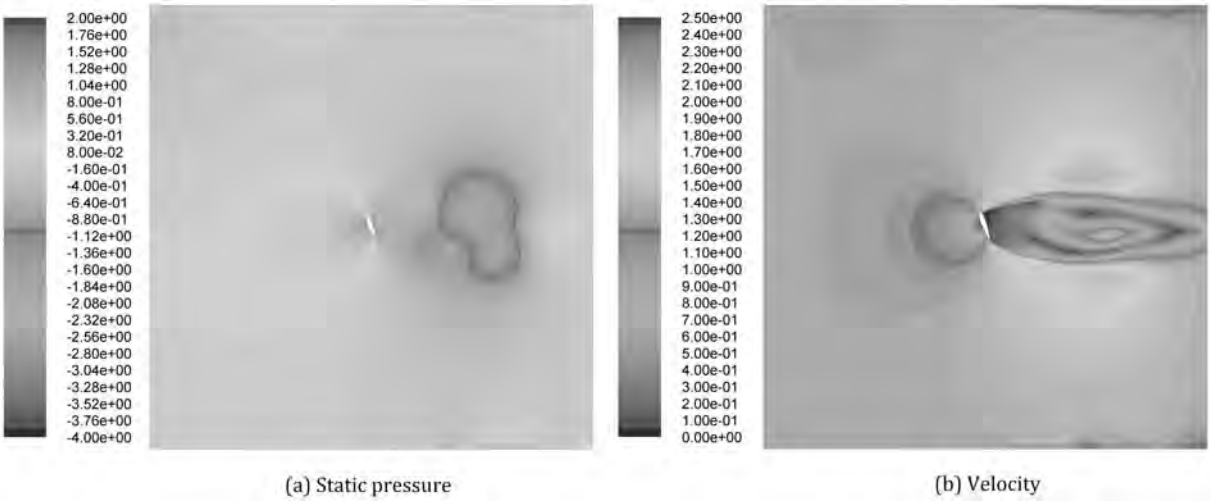

Fig. 7 Flow around a NACA section at $H/C = 15$ and AoA of 70° (open)

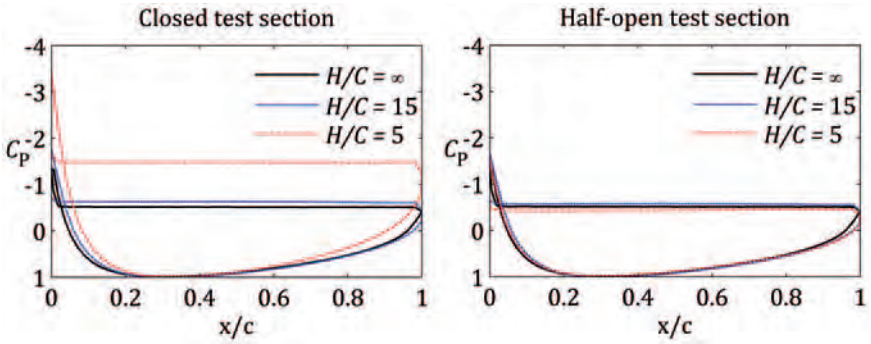

Fig. 8 C_P comparison of closed and half-open test sections at AoA of 70°

between the high H/C closed test section and the corresponding half-open section. However, at the lower H/C ratio, very substantial errors are observed in the closed section pressures, particularly on the downstream suction side of the blade. On the pressure surface, all three cases demonstrate an almost constant static pressure over most of the surface, but the magnitude of this negative pressure coefficient is almost doubled as a consequence of wall interaction in the closed section, low H/C case. The clear implication of these results is that wind tunnel testing must be performed either in half-open test sections or in closed sections with very high H/C ratio. For the study described here, a half-open test section was adopted.

To suit the test section, the aerofoils were designed to have a span of 0.450 m and a chord of 0.11 m, resulting in both section H/C ratio and the aerofoil aspect ratio having a value of 4.1. Initial CFD evaluation confirmed that this test configuration resulted in a 2-D flow over much of the aerofoil's span while retaining a large-enough cross-section to contain the required internal instrumentation. The aerofoils were produced by rapid prototyping from Fullcure 720 material giving a high surface precision (±0.1 mm).

Pressure tappings were located at midspan to measure the nominally 2-D pressure coefficient. Each aerofoil had different pressure tapping locations depending on the shape and local thickness of the aerofoil. The number of pressure tappings were 24, 22, 30, and 32 for NACA0012, SG6043, SD7062, and DU06-W-200, respectively. All tappings were connected to a 48-channel Scanivalve. The models were cantilevered from a Plint electronic force balance that was mounted on one side of the test section and which had been modified to provide an analogue output signal for each force component.

A computer-based system was used to record all pressure and force signals via an NI USB-6218 ADC consisting of 16 channels with a resolution of 16 bits. This device has a sample rate of up to 250 kS/s.

All forces were measured at a rate of 800 Hz and averaged over a period of 2.5 s. Forces were measured for the full 360° incidence range in 2° increments (except for the symmetric NACA0012 which was measured over 180°).

The static pressure measurements on each aerofoil were obtained through the computer-controlled Scanivalve using the same sampling rate and frequency. Measurements on the aerofoils were obtained at three Reynolds numbers (nominally 65 000, 90 000, and 150 000).

3 AEROFOIL PERFORMANCE CHARACTERISTICS

A series of lift, drag, and pressure coefficients are presented in this section. The measured pressure coefficients are presented alongside numerical predictions generated by the FLUENT commercial software.

3.1 NACA0012

Figures 9 and 10 show the lift and drag coefficient curves for the NACA0012 section at three tested Reynolds numbers and, as expected, it can be seen that the lift curves in pre-stall are not significantly affected by the Reynolds number. The maximum lift coefficients occur at 12° angle of attack for all Reynolds numbers, but the peak lift coefficient is seen to increase with Reynolds number to maxima of 0.778, 0.781, and 0.816 for the three tested Reynolds numbers. This maximum lift is comparable to the value of 0.853 measured by Sheldahl and Klimas [**19**] at the higher Reynolds number of 160 000.

With further small incidence increase, the flow separates over the entire aerofoil surface and the lift

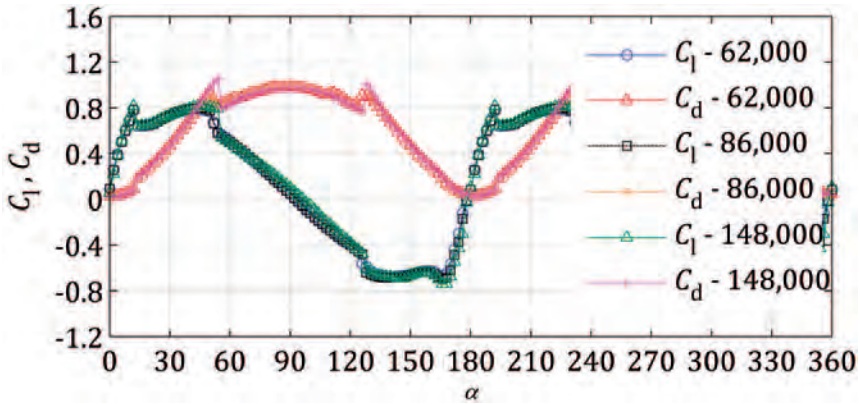

Fig. 9 Lift and drag coefficients: NACA0012

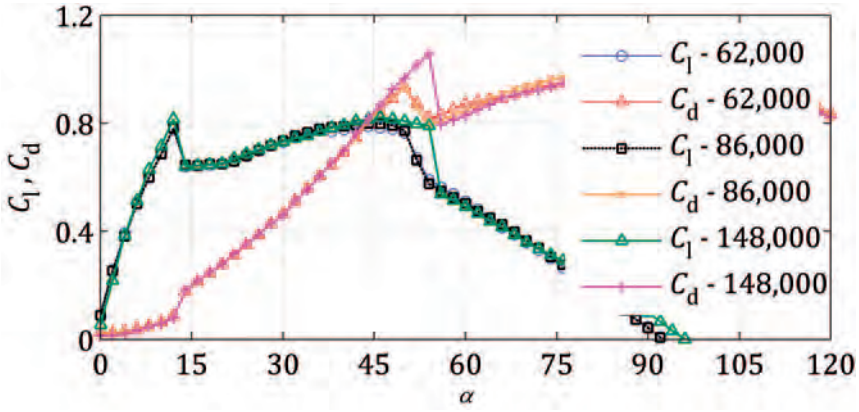

Fig. 10 Lift and drag coefficients: NACA0012 (close-up)

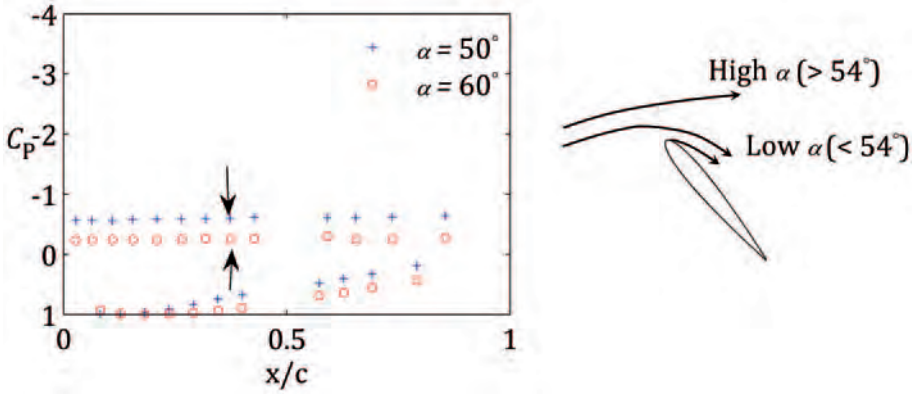

Fig. 11 Surface static pressure coefficients and flow schematic

drops rapidly to a value of approximately 0.64 before gradually increasing again to 0.8 at around 45°. There is a further sudden drop in lift at 54°, followed by further gradual reduction to zero at 90°. Static pressure measurements either side of 54° reveal that the fall in lift corresponds to a sudden change of flow behaviour, particularly on the suction side. Figure 11 shows the variation of pressure coefficient with distance from the leading edge. As expected, in this stalled flow, the suction side pressure remains almost constant over the entire surface, but there is a very significant change in the magnitude of that pressure coefficient between 50° and 60° incidence. When the AoA is <54°, the flow remains attached over the first few millimetres of the leading edge, which is sufficient to cause substantial turning of the flow before separation occurs. Above 54° incidence, the flow separates immediately as though over a flat plate, resulting in deflection of the opposite sign (shown schematically in Fig. 11). The latter flow regime induces lower air movement (lower velocity) on the suction surface and, hence, higher (or less negative) pressure coefficient.

These trends, including the pressure coefficient discontinuities, are reversed as the AoA passes 90° and the aerofoil is, in effect, travelling backwards.

In terms of drag, the usual pre-stall trend is followed as the angle of attack increases. It is also seen that drag coefficients decrease slightly with increasing Reynolds number. Drag then increases sharply at the stall point, corresponding to the observed reduction in lift, and continues to increase rapidly to a peak at approximately 54°. Further incidence increase results in a rapid fall in drag, again corresponding to an observed discontinuity in the lift curve at that incidence. Although the peak drag magnitude appears to be Reynolds number sensitive, all three tests show a fall to about the same value of drag coefficient (0.8). The drag then increases again reaching a second peak at 90°. Above 90°, the trend is reversed.

Figure 12 presents CFD-derived and experimental pressure coefficients for NACA0012 and it is seen that at modest incidences (e.g. 5°), the CFD captures the experimental results well as might be expected. However, as stall is approached, the wind tunnel

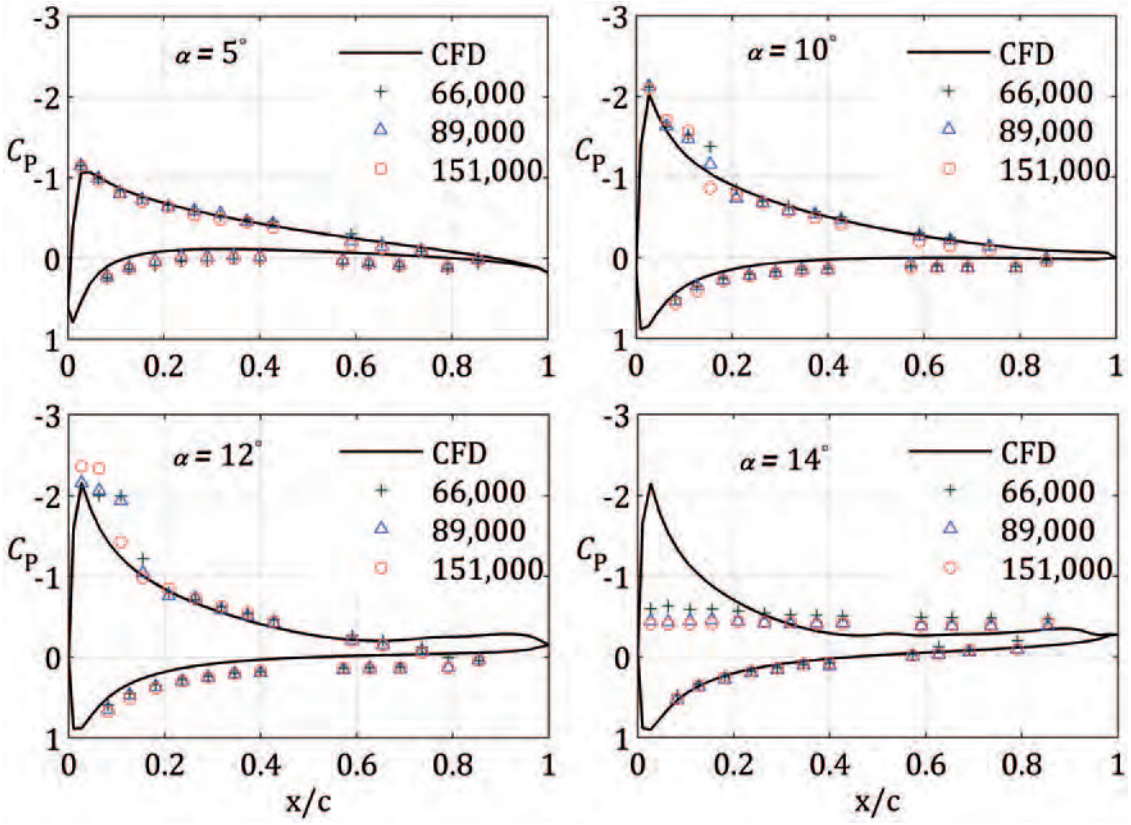

Fig. 12 Pressure coefficients: NACA0012

data reveal a suction surface separation bubble in the diffusing zone immediately downstream from the suction peak which is not captured by the CFD (AoA 10° and 12°). At 14° incidence, the aerofoil is completely stalled. Reynolds number does not have a profound effect on the C_P characteristics except in the formation of the laminar separation bubbles. In each case, the laminar separation occurs in the rapidly diffusing flow at around 5 per cent chord, moving slightly upstream with increasing angle of attack. Turbulent reattachment occurs at around 20 per cent chord. By 14° incidence, full stall has occurred, which is thought to be caused when the flow that is separated by the bubble can no longer sustain turbulent reattachment due to low energy in the flow; a process known as bubble bursting [**24**]. This results in a sudden stall with relatively sharp lift peak (as can be seen from the force measurements (Fig. 9)). This is not captured by the CFD prediction in which formation of the bubble is not predicted and stalling is a result of a gradual separation that is initiated at the trailing edge. The stalling angle of attack is 14° for all three of the tested Reynolds numbers. A summary of the positions of separation, reattachment, and bubble size for NACA0012 is presented in Fig. 13. There is no significant difference in the laminar separation point for different Reynolds numbers, but the reattachment process takes place more rapidly at higher Reynolds number.

3.2 SG6043

The SG6043 aerofoil exhibits both a higher peak lift and a slightly more progressive and delayed stall relative to NACA0012 (Fig. 14). In this case, the stall characteristic is a combination of trailing-edge stall and leading-edge stall. A trailing-edge separation advances progressively upstream with increasing incidence, as can be seen from the static pressure distributions (Fig. 15). It should be noted that although measurements were not possible very close to the trailing edge because of insufficient blade thickness to accommodate the instrumentation, the agreement between the measurements and CFD over the blade surfaces approaching the trailing edge give confidence in the use of CFD predictions in this zone. In addition to trailing-edge separation, a separation bubble is also seen which moves towards the leading edge with increasing AoA. The surface static pressure distribution at 16° incidence angle shows that trailing-edge separation covers around 30 per cent of the blade's suction surface when the bubble reaches the leading edge. Further incidence increase lead to bubble bursting. The consequence

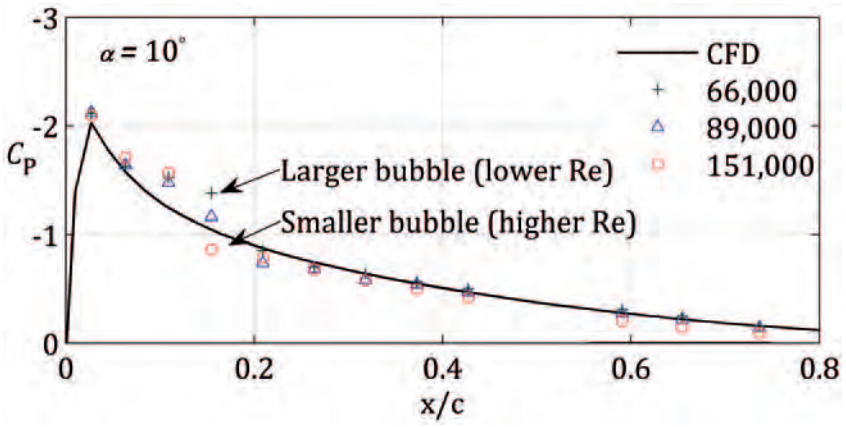

Fig. 13 Separation and reattachment: NACA0012 suction surface

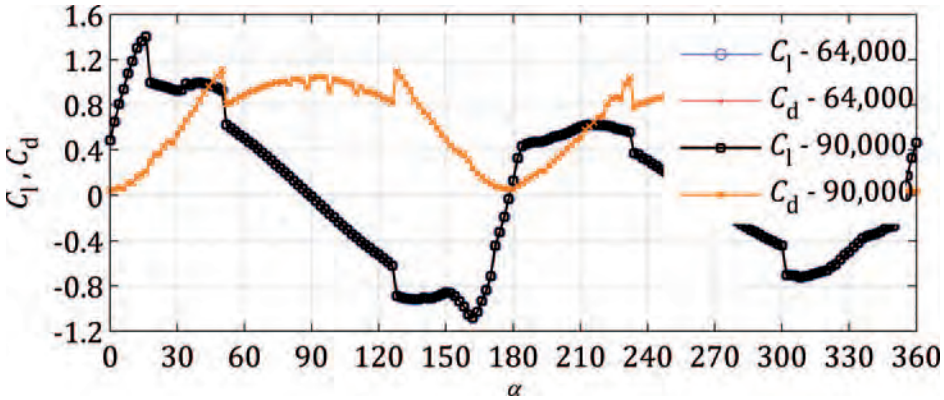

Fig. 14 Lift and drag coefficients: SG6043

of these two different simultaneous stall mechanisms is an initially progressive stall as the trailing edge stall develops, followed by an abrupt loss of lift when the leading edge bubble bursts. The maximum values of lift for this aerofoil at the three, increasing test Reynolds numbers are 1.358, 1.403, and 1.431 at respective incidence angles of 16°, 16°, and 18°. After the stall point, the lift drops to a value of around 0.97. A comparison of the surface static pressure distributions of NACA0012 and SG6043 (Figs 12 and 15) shows that SG6043 produces a consistently larger pressure difference between the suction and pressure surfaces even when fully stalled. This is mostly due to the effect of camber that leads to an increased lift contribution from the pressure surface.

Like NACA0012, the lift coefficient remains relatively constant with further increase in angle of attack up to approximately 50°, where a second rapid fall in lift occurs followed by a further, almost linear fall to zero lift at the 90° incidence point. A similar but reversed characteristic is mirrored beyond 90°, but it should be noted that unlike the symmetrical NACA0012, the lift characteristic on either side of 90° incidence is no longer perfectly symmetrical. The drag characteristic is almost identical to that of the previously described NACA0012.

Further analysis of the static surface pressure distributions for this aerofoil shows that relative to the NACA section, the bubble is first detected at a higher angle of attack (12°). Trailing-edge separation is first seen at 14° incidence as indicated by a nearly constant pressure and full stall is observed at an angle of attack of 18° when the bubble reaches the leading edge and bursts.

3.3 SD7062

The lift characteristics of the SD7062 aerofoil are shown in Fig. 16 and it can be seen that it closely resembles that of the SG6043 profile. As the Reynolds number is increased, the maximum lift coefficients of 1.163, 1.354, and 1.397 occur at the respective angle of attack of 14°, 16°, and 18°. The

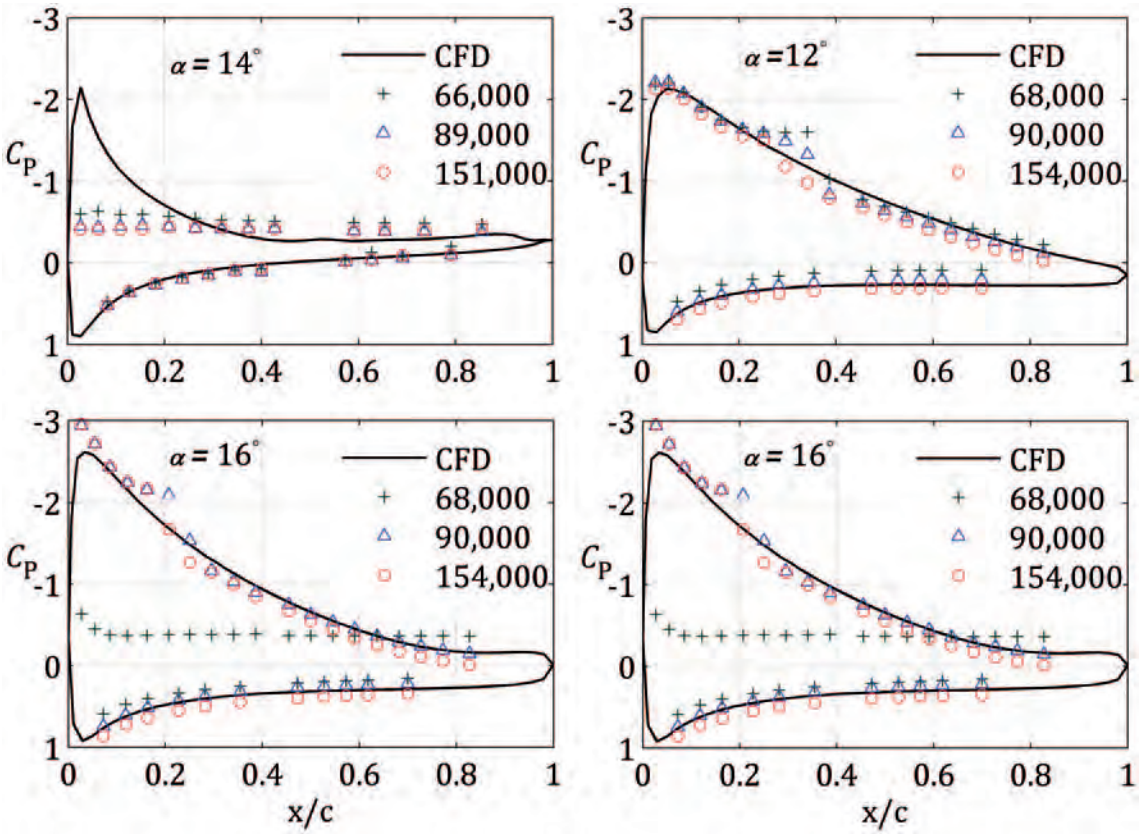

Fig. 15 Pressure coefficients: SG6043

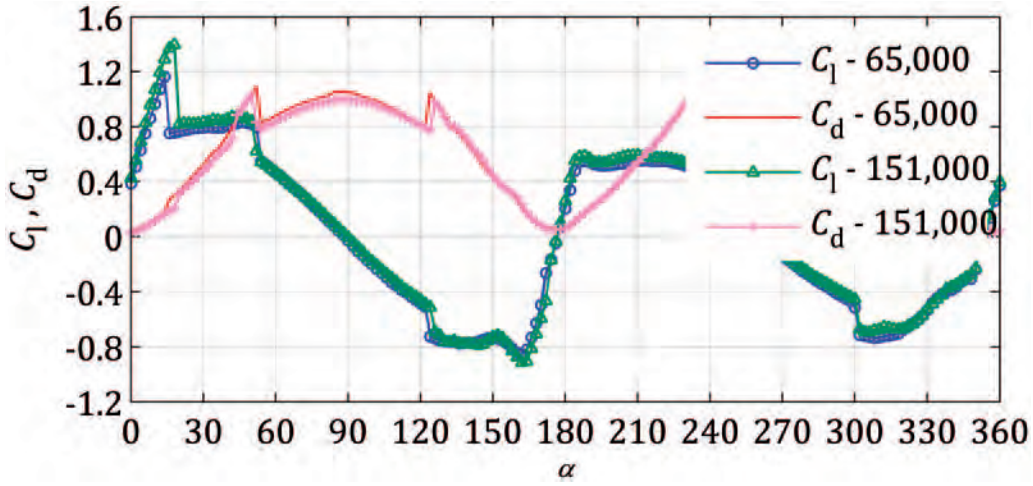

Fig. 16 Lift and drag coefficients: SD7062

post-stall values of the lift coefficient for this aerofoil are around 0.8 which is a little bit lower than for SG6043. The drag coefficients are again similar to both of the previously presented cases.

The SD7062 aerofoil section also demonstrates the presence of a laminar separation bubble which is first seen at 12° angle of attack (Fig. 17). However, the separation bubble differs from the previous two cases in that it occurs further downstream at about 20 per cent chord and that the length of the bubble seems to be much more sensitive to Reynolds number. At the highest tested Reynolds number, the layer reattaches almost immediately, but for the lowest Reynolds number, reattachment does not occur until around 40 per cent chord. The bubble's separation point moves forward to the leading edge with further increase in AoA. Full stall is first observed at 16° incidence at the lowest Reynolds number (68 000), whereas at the highest Reynolds number, stall is delayed to 20° incidence.

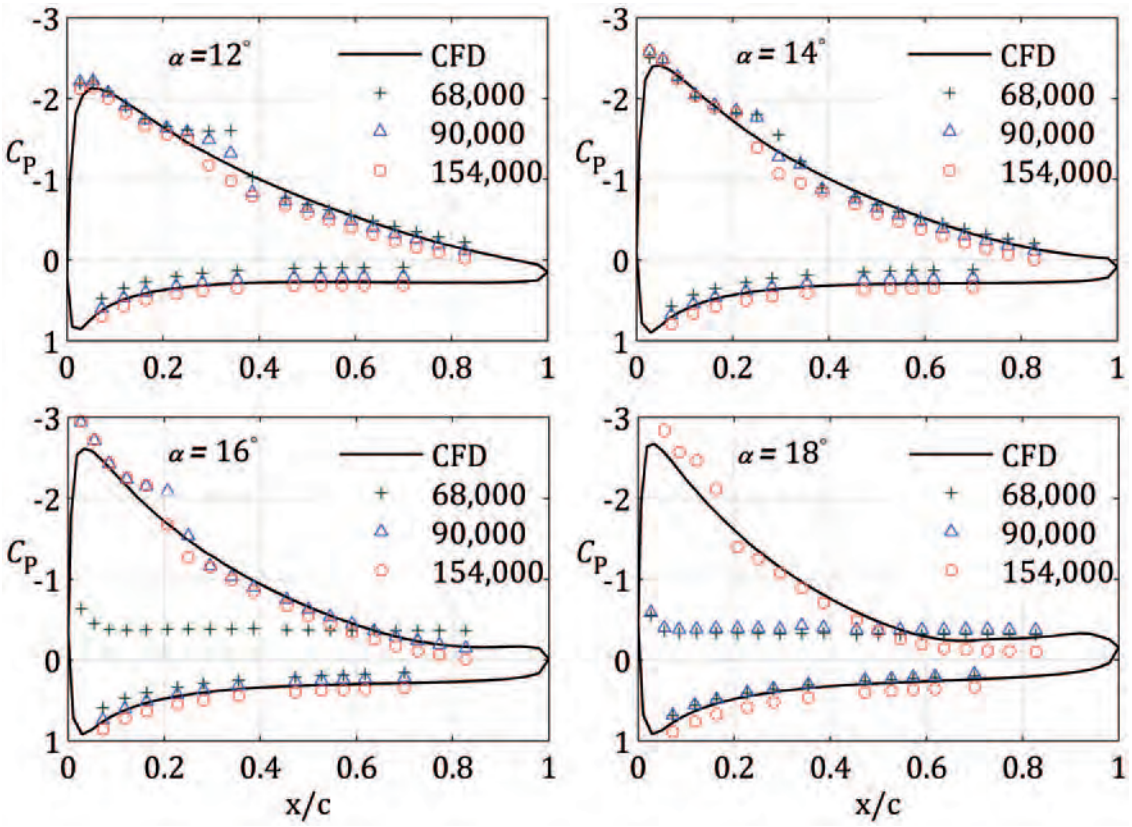

Fig. 17 Pressure coefficients: SD7062

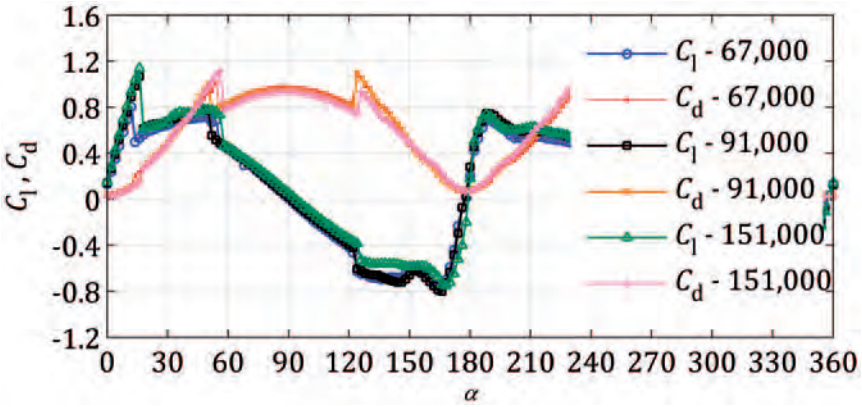

Fig. 18 Lift and drag coefficients: DU06-W-200

3.4 DU06-W-200

Figure 18 presents the lift characteristics of DU06-W-200. The maximum pre-stalled lift coefficients with progressively increasing Reynolds number are 0.804, 1.067, and 1.136, but it can be seen that the lift production of this aerofoil is more sensitive to the Reynolds number than the previous three aerofoils. For instance, when the Reynolds number is reduced from 151 000 to 68 000, a lift coefficient reduction of almost 0.33 is seen. Lift generation at higher angles of attack is similar to that of NACA0012.

The surface pressure distributions (Fig. 19) again reveal the formation of separation bubble which is observed to form at moderate AoA and which moves forward towards the leading edge and reduces in length as the angle of attack increases. At the lowest Reynolds number, the aerofoil stalls at 14°.

In the light of these experimental results, it can be seen that SG6043 and SD7062 exhibit relatively higher

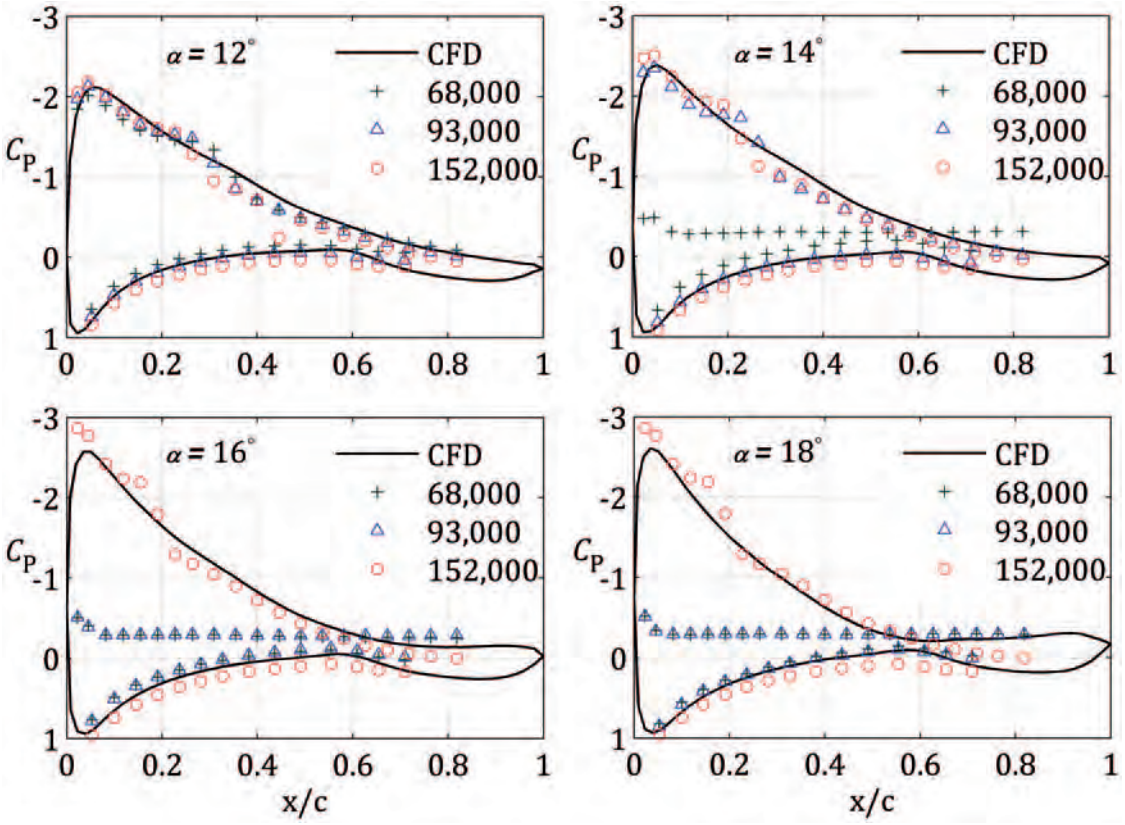

Fig. 19 Pressure coefficients: DU06-W-200

pre-stall lift coefficient peaks (around 1.4) and outperform the others at all incidence angles from 0° to 90°. Significantly, for the wind turbine applications, their higher lift characteristics in the post-stall region make them well suited for horizontal-axis applications for which incidence angles experienced by the turbine blades are frequently in this range.

Performance comparisons between NACA0012 and DU06-W-200 show that the latter can produce a higher lift peak at the highest tested Reynolds number but suffers from performance degradation with decreasing Reynolds number. This, combined with its comparatively high thickness ratio which contributes to a higher moment of inertia, suggests that DU06-W-200 is less suitable for a turbine operating predominantly in a relatively low-wind environment in which the self-starting problem is of concern.

It is also observed that, although SG6043 and SD7062 lose their performance advantage at very high incidence (180° to 360°), their degraded performances remain comparable to those of NACA0012 and DU06-W-200 (Fig. 20), suggesting that these high-camber aerofoils might be used with vertical-axis applications to improve rotor performance.

4 COMPARISON WITH PREVIOUS WORK: THE NACA0012 CASE

Probably, the most well-documented and widely adopted data for high incidence wind turbine applications is that of Sheldahl and Klimas [**19**]. In this section, the measured lift and drag coefficients from this study at the highest tested Reynolds number (148 000) are compared to their data at the relatively similar Reynolds number of 160 000. Despite the widespread use of this particular set, it must be noted that Sheldahl and Klimas conducted measurements at only three Reynolds numbers (360 000, 500 000, and 700 000) and consequently the results that they published for other Reynolds numbers were obtained through extrapolations. It is also noted that their tests were conducted in a closed test section wind tunnel with height-to-chord ratio of 14. Figure 21 compares the results.

In terms of lift coefficient, relatively good agreement is seen between the two sets of data in the pre-stall regime. Both give almost identical lift coefficient peak values, although the Sheldahl and Klimas data show a very slightly earlier stall. Immediately after the stall, the lift coefficient from the current study falls to a value of around 0.6, maintaining and

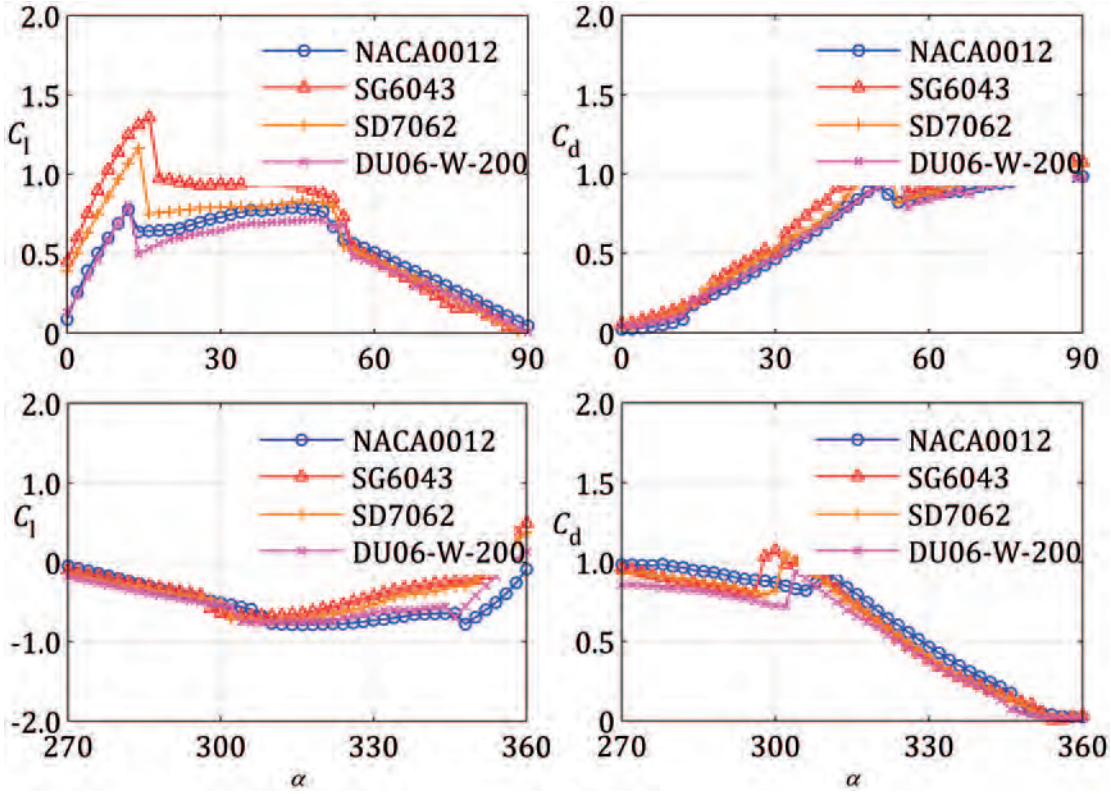

Fig. 20 Performance comparisons

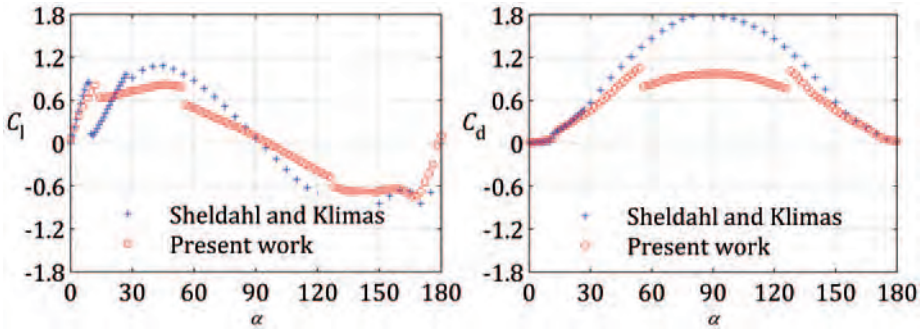

Fig. 21 Lift and drag comparisons

gradually increasing that value with increasing AoA to 54°. The Sheldahl lift curve shows a quite different post-stall characteristic in which the lift coefficient suddenly drops to almost zero before sharply rising to the second peak of around 1.1 C_l. It is not clear what physical flow mechanism could result in such a dramatic lift loss and recovery in the immediate post-stall zone and it is unfortunate that this feature was not discussed by Sheldahl and Klimas in their original work. Examination of static pressure coefficients at the stall angle (Fig. 12) reveals that when the AoA changes from 12° to 14°, although there is a loss of pressure on the suction side, the static pressure coefficients on the pressure side do not change dramatically and there still exists a pressure difference. It seems improbable that such a low value of lift (0.1) will occur at the stall angle.

Lift from both tests then gradually reduces to around zero at 90° AoA, although the Sheldahl data does not exhibit the discontinuity at 54° that has been observed in this study.

In terms of drag, good agreement is again seen in the pre-stall region and, perhaps surprisingly, the drag results are similar too in the post-stall zone up to almost 60, despite the significant differences in the observed lift characteristics.

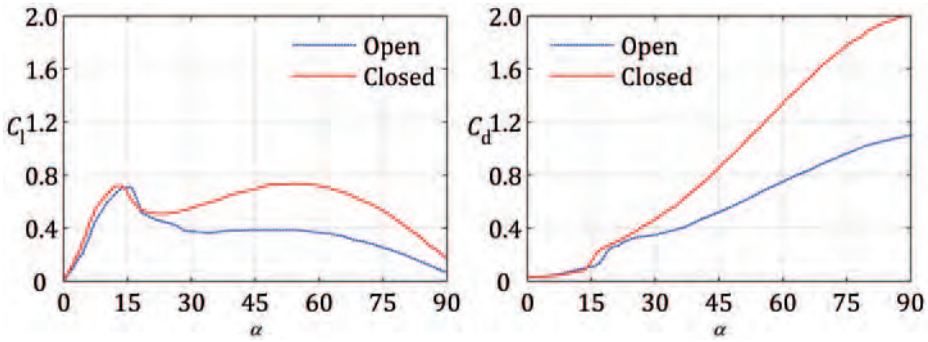

Fig. 22 Closed and open test section aerodynamic data of NACA0015 (from Rainbird [17])

Another important difference between the two data-sets is the second lift peak behaviour (i.e. the peak of lift coefficient that occurs close to 45° incidence. Here, the results of Sheldahl and Klimas [**19**] show a very clear peak that even exceeds the measured maximum pre-stall lift, while only a slight increase in lift is seen in this work.

A similar discrepancy was first examined by Rainbird [**17**] who undertook a broad review of published aerofoil performance data and found it to be inconsistent, especially post-stall. The data can be categorized into two clear groups: those that display a distinct, high second lift peak and those that do not. He hypothesized that it might be an effect of the test section configuration used in the experiments and by conducting his own tests using both closed and open test sections, he found that he could replicate both of the alternative lift characteristics simply by changing the test section configuration. Figure 22 illustrates his results.

It can be seen from the results that the test with a closed test section managed to replicate the Sheldahl trend for both lift and drag coefficients. It has already been shown that closed section measurements are strongly affected by wall proximity. While the lift coefficient of the open test section is nearly constant in the post-stall region, the lift coefficient from the closed test section rises to the second peak. For drag coefficient, it appears that drag from the closed test section is higher than that of open test section in the post-stall region. The difference is more pronounced with increasing AoA and at 90°, the drag coefficient from the closed test section is nearly double that of the open test result. In light of this information, the data of Sheldahl and Klimas and others who performed their high-incidence measurements at low H/C ratio must be viewed with some caution.

Rainbird's [**17**] force measurements are consistent with the CFD simulation results that were presented in Fig. 8, which show that there is a substantial reduction of pressure on the suction side of the aerofoil at high incidence which leads to a significant increase in the pressure difference contributing to higher lift and drag. It appears that the closed test section confines and significantly alters the flow around the aerofoil leading to increased acceleration and high velocity in the vicinity of the leading and trailing edges, leading to lower pressure on the suction side and, hence, the second lift peak behaviour.

It is worth noting that the observed change in lift and drag at around 50° angle of attack that has been reported in this study was not seen in Rainbird tests which is thought to be a consequence of the higher Reynolds numbers that were investigated by Rainbird ($Re \sim 200\,000$).

5 POST-STALL COMPARISONS WITH THE AERODAS MODEL

Post-stall comparisons between this wind tunnel data and the lift and drag prediction from the most recent stall model developed by Spera (named AERODAS) [**12**] have been made to check the ability of that model to predict aerodynamic data under these conditions. The comparisons are made for one Reynolds number (90 000). Since aerodynamic coefficients in the pre-stall region are almost linear and normally well predicted, only post-stall data (from 20° to 90°) are presented here (Fig. 23).

The comparisons demonstrate significant differences between predictions by the AERODAS model and experimental results. Lift predicted by the model always increases to a second peak at around 40° and then gradually reduces to around zero at 90°, while post-stall measured lifts behave differently (nearly constant post-stall lift). Discrepancies between predicted and measured drag coefficients are seen for all angles of attack and they are more pronounced with increasing incidence angle. The maximum predicted drag is about 2 at 90°.

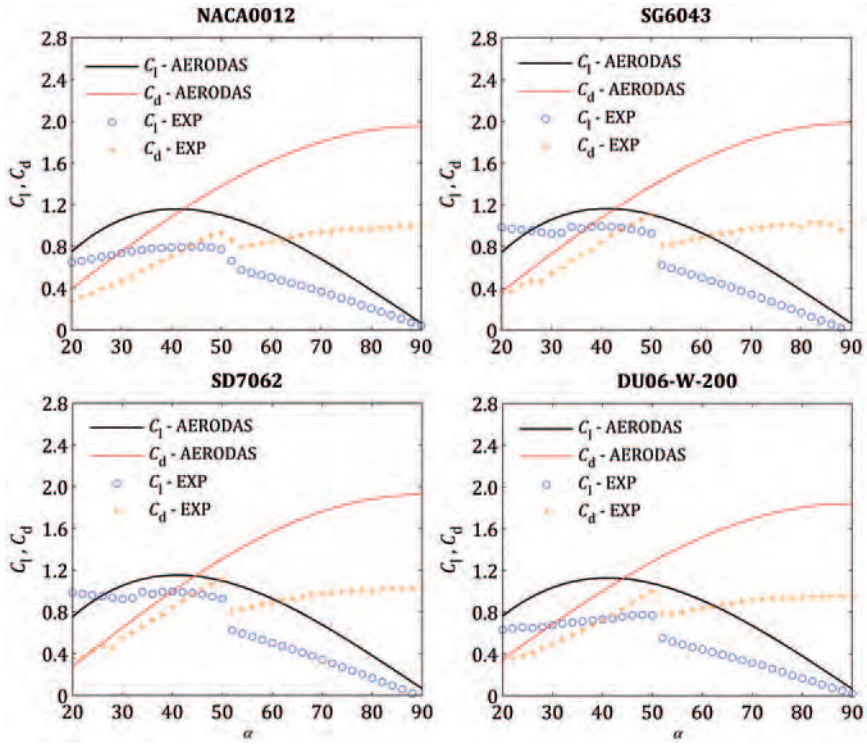

Fig. 23 Post-stall comparisons between measurements and the AERODAS model

The discrepancies are mainly due to the source of high-incidence-angle aerofoil data used in the correlation that were obtained from Ostowari and Naik [**13**, **14**]. Their measurements were made in a closed test section wind tunnel having a height-to-chord ratio of only 10; a ratio that is inadequate according to Rainbird's hypothesis.

6 CONCLUSIONS

Four aerofoils have been experimentally investigated at low Reynolds number for the full incidence range of 360°. At these Reynolds numbers, all four aerofoils demonstrate the formation of a leading-edge separation bubble that ultimately bursts leading to sudden stall. The most highly cambered aerofoils exhibit a simultaneous trailing-edge separation that advances upstream with increasing incidence, resulting in a more progressive stall characteristic, but it is always the bursting of upstream bubble that leads to a fully stalled flow. After stall, the lift drops to a sustained but lower value, the magnitude of which is dependent upon aerofoil geometry. For the symmetrical and low-camber aerofoils, the lift then rises gradually to a second peak at about 50° incidence, but this increase is less apparent for the higher camber sections.

The benefits of increased lift and more progressive stall from the cambered aerofoils are partly negated by a loss of performance arising from their 'reversed' camber when they operate in an incidence angle of 180° to 360°. The drag characteristics of all four geometries are comparable.

A comparison between these new data and the widely used Sheldahl and Klimas' data for the NACA section shows good agreement for the pre-stall region but discrepancies are observed in the deep-stall region that are consistent with Rainbird's hypothesis regarding the influence of wind tunnel test section geometry; a result that is confirmed by CFD modelling. In light of this, previous test data obtained from closed test sections should be viewed with caution, especially at high incidence angles.

Comparisons of post-stall characteristics demonstrate discrepancies between wind tunnel data and AERODAS predictions. The discrepancies confirm the need for more high-quality, low-Reynolds-number, and high-angle-of-attack data and the need for model improvements.

FUNDING

This work was supported by Royal Thai Government Scholarship.

ACKNOWLEDGEMENTS

The authors acknowledge Phillip Duffy for his work on aerofoil rapid prototyping. The assistance of Colin Wintrip and Roger Little in setting up the wind tunnel is greatly acknowledged.

REFERENCES

1 **Wilson, R.** and **Lissaman, P.** *Applied aerodynamics of wind power machines*, 1974 (State University, Oregon).
2 **Wilson, R., Lissaman, P.,** and **Walker, S.** *Aerodynamic performance of wind turbines*, 1976 (State University, Oregon).
3 **McCarty, J.** *PROP93 Users guide*, 1993 (Alternative Energy Institute).
4 **Buhl, M.** *WTPERF Users guide*, 2000 (National Renewable Energy Laboratory).
5 **Moriarty, P.** and **Hansen, A.** *Aerodyn theory manual*, 2005 (NREL/CP-500-36900, National Renewable Energy Laboratory).
6 **Simms, D., Shreck, S., Hand, M.,** and **Fingersh, L.** *NREL unsteady aerodynamics experiment in the NASA-Ames wind tunnel: A comparison of prediction to measurements*, 1999 (NREL/TP-500-29494, National Renewable Energy Laboratory).
7 **Tangler, J.** *The nebulous art of using wind-tunnel airfoil data for predicting rotor performance: preprint*, 2002 (NREL/CP-500- 31243, National Renewable Energy Laboratory).
8 **Hill, N., Dominy, R., Ingram, G.,** and **Dominy, J.** Darrieus turbines: the physics of self-starting. *Proc. IMechE, Part A: J. Power and Energy*, 2008, **223**, 21–29.
9 **Viterna, L.** and **Corrigan, R.** *Fixed pitch rotor performance of large horizontal axis wind turbines*, 1982 (DOE/NASA Workshop on Large Horizontal Axis Wind Turbines, Cleaveland, Ohio).
10 **Lindenburg, C.** *Stall coefficients: Aerodynamic airfoil coefficients at large angles of attack*, 2001 (ECN-RX-01-004, ECN).
11 **Laino, D.** Foilcheck: A utility for creating aerodynamic input files for AeroDyn-based program, National Renewable Energy Laboratory Lecture notes, 2005.
12 **Spera, D.** *Models of lift and drag coefficients of stalled and unstalled airfoils in wind turbines and wind tunnels*, 2008 (NASA/CR- 2008-215434, NASA).
13 **Ostowari, C.** and **Naik, D.** Post stall studies of untwisted varying aspect ratio blades with an NACA4415 airfoil section - Part 1. *Wind Eng.*, 1984, **8**(3), 176–194.
14 **Ostowari, C.** and **Naik, D.** Post stall studies of untwisted varying aspect ratio blades with an NACA44xx airfoil section - Part 2. *Wind Eng.*, 1985, **9**(3), 149–164.
15 **Timmer, W.** and **van Rooij, R.** The performance of new wind turbine blade tip and root airfoils up to high angles-of-attack, Delft University of Technology. In Proceedings of the *2001 European wind energy conference*, July 2001, Copenhagen. pp. 2–6.
16 **Wright, A.** and **Wood, D.** The starting and low wind speed behaviour of a small horizontal axis wind turbine. *J. Wind Eng. Indl. Aerodyn.*, 2004, **92**, 1265–1279.
17 **Rainbird, J.** *The aerodynamics development of a vertical axis wind turbine*. Master's thesis, School of Engineering, University of Durham, 2007.
18 **Rozhdestvensky, K.** Wing-in-ground effect vehicles. *Prog. Aerosp. Sci.*, 2006, **42**(3), 211–283.
19 **Sheldahl, R.** and **Klimas, P.** *Aerodynamic characteristics of seven symmetrical airfoil sections through 180-degree angle of attack for use in aerodynamic analysis of vertical axis wind turbines, SAND80-2114*, 1981 (National Renewable Energy laboratory).
20 **Selig, M.** Low reynolds number airfoil design, Lecture notes, 2003.
21 **Selig, M.** Summary of low-speed airfoil data, [Internal] Technical report, SoarTech Publication, 1997.
22 **Claessens, M.** *The design and testing of airfoils for application in small vertical axis wind turbines*. Master's thesis, Faculty of Aerospace Engineering, Delft University of Technology, 2006.
23 **Mueller, T. J.** and **DeLaurier, J. D.** Aerodynamics of small vehicles. *Annu. Rev. Fluid Mech.*, 2003, **35**, 89–111.
24 **Lissaman, P.** Low-reynolds-number airfoils. *Annu. Rev. Fluid Mech.*, 1983, **15**, 223–239.

APPENDIX

Notation

AoA	angle of attack
C	aerofoil chord
C_d	drag coefficient
C_l	lift coefficient
C_P	pressure coefficient
H	test section height
Re	Reynolds number